Journal of Modern Optics

ISSN: 0950-0340 (Print) 1362-3044 (Online) Journal homepage: http://www.tandfonline.com/loi/tmop20

Direct multi-level density matrix calculation of nonlinear optical rotation spectra in rubidium vapour

Nikolai Korneev & Olena Benavides

To cite this article: Nikolai Korneev & Olena Benavides (2009) Direct multi-level density matrix calculation of nonlinear optical rotation spectra in rubidium vapour, Journal of Modern Optics, 56:10, 1194-1198, DOI: 10.1080/09500340902990023

To link to this article: https://doi.org/10.1080/09500340902990023

Journal of Modern Optics
Vol. 56, No. 10, 10 June 2009, 1194–1198

Taylor & Francis
Taylor & Francis Group

Direct multi-level density matrix calculation of nonlinear optical rotation spectra in rubidium vapour

Nikolai Korneev[a]* and Olena Benavides[b]

[a]*Instituto Nacional de Astrofisica, Optica y Electronica, Apt. Postal 51 y 216, CP 72000, Puebla, Pue., Mexico;* [b]*Universidad Autonoma del Carmen, Cd. del Carmen, Campeche, Mexico*

(*Received 6 March 2009; final version received 22 April 2009*)

We propose a rapid solution algorithm for the calculation of the full density matrix evolution for a multi-level atom. The calculation principle is similar to the split-step algorithm widely used for modelling the nonlinear propagation in media with Kerr-type nonlinearity, optical fibres in particular. The spectrum of nonlinear Faraday rotation in the D_2 natural rubidium line is calculated and compared with the experiment. Good agreement is obtained.

Keywords: Faraday rotation; rubidium; density matrix

1. Introduction

Laser light interaction with rubidium vapour is important for applications as well as from the fundamental viewpoint. If the CW laser is tuned directly into a resonance, strong nonlinear effects arise; absorption and refraction can depend on laser intensity, polarisation state and external magnetic field. In particular, nonlinear Faraday rotation is observed [1], which can be used for magnetometry and for efficient hologram writing [2].

For open transitions in rubidium the weak-probe linear limit holds only for intensities as low as $I_0 \approx 10^{-3}\, I_{\mathrm{sat}}$, with saturation intensity $I_{\mathrm{sat}} \approx 1\text{–}3\,\mathrm{mW\,cm^{-2}}$ [3]. The absorption and refraction strongly depend on the beam diameter (time of transit). The theory for the nonlinear regime is complicated because of the big number of sublevels involved (Figure 1). The established method of theoretical description in this case is the master equation for the atomic density matrix [5–7], but for a large number of sublevels the calculations become very time-consuming. Since the steady state is not attained for open transitions during the time of transit, for realistic calculations it is highly desirable to take into account the whole temporal evolution of atomic parameters.

Instead of solving for full evolution it is possible to introduce an effective repopulation for lower levels and to take an effective steady state. This simplifies the solution, but the repopulation parameters are not obtained directly, and have to be fixed according to experiment [8]. Even with the fitting parameters, the agreement with experiment in [8] is not very good. The Monte Carlo methods were proposed, which can in principle make the solution for multi-level atoms faster [7,9], but practical application of them to rubidium is complicated, because a large number of runs is necessary to reduce the statistical error. We propose here the direct numerical method, which produces a rapid enough solution of complete dynamics for the master equation of a multi-level rubidium atom with good exactitude. Such a solution does not contain free parameters. The calculation principle is similar to the split-step algorithm widely used for modelling the nonlinear propagation in media with Kerr-type nonlinearity, optical fibres in particular [10]. The results agree quite well with experimentally observed spectra.

2. Solution principle

The evolution master equation is written as [6,7]

$$\frac{\partial \rho}{\partial t} = (\mathrm{i}/\hbar)[\rho, H] + \sum_{q=-1,0,1} C_q \rho C_q^{+} - \frac{1}{2}(C_q^{+} C_q \rho + \rho C_q^{+} C_q), \tag{1}$$

where ρ is density matrix, H is the Hamiltonian of a free atom, and C_q, C_q^{+} are lowering and raising

*Corresponding author. Email: korneev@inaoep.mx

ISSN 0950–0340 print/ISSN 1362–3044 online

DOI: 10.1080/09500340902990023
http://www.informaworld.com

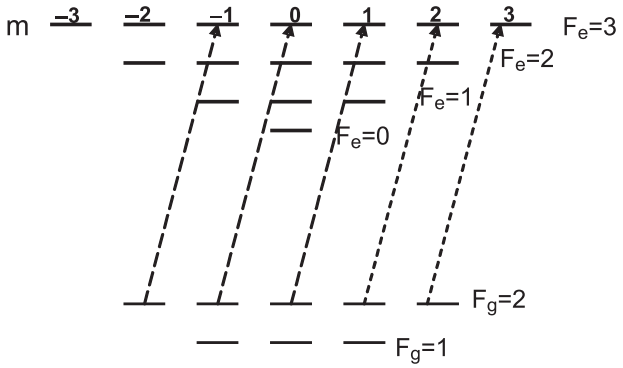

Figure 1. Energy levels for ^{87}Rb transition D_2 (not to scale). Dashed lines are transitions induced by the light of circular polarisation in resonance with $F_g = 2$, $F_e = 3$. For ^{85}Rb, all F numbers are bigger by 1, the m numbers change accordingly. The detailed data on transitions can be found in the online reference [4].

atomic operators:

$$\begin{aligned} C_q^+ \left| F_g, m_{F_g} \right\rangle &= \Gamma^{1/2} (1, F_g, q, m_{F_g}; F_e, m_{F_e} \\ &\quad = m_{F_g} + q) \left| F_e, m_{F_e} = m_{F_g} + q \right\rangle, \\ C_q^+ \left| F_e, m_{F_e} \right\rangle &= 0, \\ C_q &= (C_q^+)^* \end{aligned} \tag{2}$$

with decay rate Γ, and Clebsch–Gordan coefficients for coupling ground and excited states' sublevels. We consider only the spontaneous emission, and do not take into account collisions because for room temperature the rubidium concentration is low ($10^{10}\,\mathrm{cm}^{-3}$), and the collision probability for the time of a beam crossing is small.

The combination

$$P = \sum_{q=-1,0,1} C_q^+ C_q \tag{3}$$

is a projector operator, its matrix has only diagonal elements $P_{kk} = P_k$.

The number of independent unknown real parameters in ρ is $N^2 - 1$ (N is the number of sublevels). For ^{87}Rb D_2 transition (870.24 nm), $N = 24$, and it is necessary to solve a system of 575 coupled differential equations. For ^{85}Rb, there are 36 sublevels, with 1295 equations. One characteristic time of this system is the lifetime Γ^{-1}. There is also a characteristic time of inverse Doppler broadening (comparable to the inverse detuning and to the inverse frequency difference between upper levels), which is 10–100 times smaller, and the time of flight of an atom through the beam, which is 10–100 times bigger. Thus, the equations, apart from a big number of variables, have quite different time scales, and conventional algorithms for ODE solution, such as Runge-Kutta, are slow and can become unstable. Additionally, averaging over Doppler-shifted groups of atoms is needed, and the system has to be solved hundreds of times for comparison with the experiment.

For solution, we note that formally Equation (1) is equivalent to

$$\frac{\partial \rho}{\partial t} = (\mathbf{A} + \mathbf{B})\rho, \tag{4}$$

where $\mathbf{A}$, $\mathbf{B}$ are superoperators corresponding to the Hamiltonian and relaxation parts, respectively. They are expressed by $N^2 \times N^2$ matrices which act on the elements of ρ treated as an N^2 vector. The formal solution of Equation (4) is given by the operator exponent:

$$\rho(t + \Delta t) = \exp((\mathbf{A} + \mathbf{B})\Delta t)\rho(t). \tag{5}$$

If each of two superoperators is treated separately, fast algorithms of calculation exist for both of them. We can more easily calculate $\exp(\mathbf{A}\Delta t)$ and $\exp(\mathbf{B}\Delta t)$, than $\exp((\mathbf{A} + \mathbf{B})\Delta t)$.

For the rotating wave approximation, when the Hamiltonian is time independent, and there is no spontaneous emission, the Hamiltonian part of evolution is given by

$$\rho(t + \Delta t) = U(\Delta t)\rho(t)U^{-1}(\Delta t) \tag{6}$$

with the unitary matrix $U(\Delta t) = \exp[-\mathrm{i}(H/\hbar)\Delta t]$.

The relaxation part of the evolution with zero Hamiltonian is calculated with:

$$\begin{aligned} \rho(t + \Delta t) &= \exp(-P\Delta t/2)\rho(t)\exp(-P\Delta t/2) \\ &\quad + \sum_{q=-1,0.1} C_q Q(t + \Delta t) C_q^+ \end{aligned} \tag{7}$$

and elements of the Q matrix are:

$$\begin{aligned} Q_{ik}(t + \Delta t) &= 2\rho_{ik}(t)(1 - \exp(-(P_i + P_k)\Delta t/2)) \\ &\quad \times (P_i + P_k)^{-1}, \end{aligned} \tag{8}$$

if $P_i + P_k \neq 0$, and $Q_{ik} = 0$ if $P_i + P_k = 0$. The derivation of Equation (7) in this form is outlined in Appendix 1.

Of course, the two operator exponents do not commute, and though the two solutions given by Equations (6) and (7) are exact, their combination is not. Nevertheless, if the time Δt is small enough, we can obtain close approximation to the exact solution by applying one matrix exponent after another.

As for the nonlinear propagation split-step, better exactitude is obtained if relaxation evolution is calculated at the middle of the time interval between the two calculations of the Hamiltonian part. It follows from the equation for linear operators:

$$\begin{aligned} \exp[(\mathbf{A} + \mathbf{B})2\Delta t] &= \exp(\mathbf{A}\Delta t)\exp(2\mathbf{B}2\Delta t)\exp(\mathbf{A}\Delta t) \\ &\quad + O\big((\Delta t)^3\big), \end{aligned} \tag{9}$$

which is related to the Baker–Campbell–Hausdorff formula. If we approximate the exponent of a sum by a simpler expression

$$\exp[(\mathbf{A}+\mathbf{B})2\Delta t] = \exp(\mathbf{A}2\Delta t)\exp(\mathbf{B}2\Delta t) + O\left((\Delta t)^2\right), \tag{10}$$

the accuracy is worse.

Since the Hamiltonian is time independent in the rotating wave approximation, the matrix exponents U, U^{-1} are calculated only once with a Taylor series, and applied consequently. The overall computation time is proportional to N^3.

From physical arguments, if we are interested in evolution over periods of time much bigger than the relaxation time, the step Δt can be safely taken to resolve only the relaxation time Γ^{-1}. This conjecture was checked for the problem of interest by comparing the solution with the exact one and by comparing solutions with different Δt. Practically, we were keeping Δt at approximately 0.1 Γ^{-1}.

We have implemented the split-step algorithm in C programming language. The calculation of a super-operator exponent with high exactitude for a limited number of sublevels was made in our earlier paper [2], and we used it for testing the program mathematics.

We are interested in the spectra for nonlinear Faraday rotation in natural rubidium in relation with our study of dynamic holography in this material. Thus, we performed the calculation and experiment for light intensity and magnetic fields typical for this application. The Hamiltonian and general data on transition were taken from the online reference [4]. Our previous calculations [2] were made in the low-field approximation for the Zeeman effect, for which the F-level splitting is linear with the magnetic field. We have found that this approximation is not sufficient for fields bigger than approximately 1 G, and the correction is more pronounced for ^{85}Rb. Thus, we used a more exact Hamiltonian, which includes the interaction with the magnetic field in the form [4]

$$H_B = \frac{\mu_B}{\hbar}(g_J J_z + g_I I_z)B \tag{11}$$

with μ_B being the Bohr magneton, J_z and I_z being the z-projections of the total electron and nuclear angular moments, with the corresponding Landé factors g_J, g_I, respectively. The z-axis is taken along the direction of the magnetic field.

For the calculations we supposed that the transitions from $F_g = 1$ and $F_g = 2$ for ^{87}Rb and from $F_g = 2$ and $F_g = 3$ for ^{85}Rb can be treated separately in the Hamiltonian because of the relatively big frequency differences between the ground levels. Of course, it is necessary to take into account both levels for the relaxation part of Equation (1). To check the validity of the approximation, for ^{85}Rb we performed partial calculations taking into account the ground level separation as well. The algorithm managed the frequency separation of $\Omega = 3.0$ GHz without any major difficulty, but the time step had to be reduced at least to 1/20 of the relaxation time to eliminate small spurious subharmonic resonances around $\Omega/3$, 4, 5 etc. The difference in the results with independent ground level approximations was comparable to the rounding errors because of finite integration intervals, and we estimate them as <0.03 of the maximal signal value. The calculation errors can be reduced by making the calculation longer (reducing time step, taking bigger intervals for time of flight and taking closer spaced points for spectra).

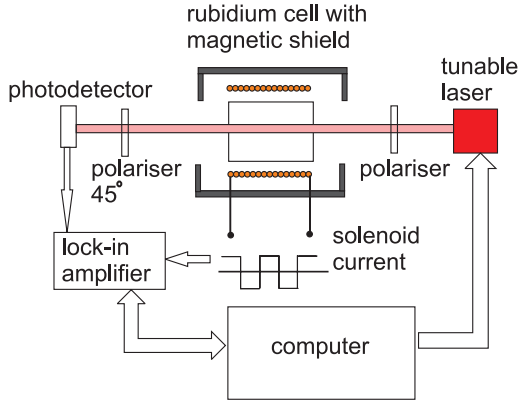

Figure 2. Experimental setup for obtaining Faraday rotation spectra. (The colour version of this figure is included in the online version of the journal.)

First we obtained the dynamics of the density matrix as a function of the detuning across the upper levels. The dipole moment evolution for left and right circularly polarised components is obtained, and averaged according to the arrival time to the centre of the beam with the Maxwell velocity distribution (see [2]). To determine the Faraday rotation, it is necessary to calculate the refractive index difference for right and left circular polarisations with the real part of the complex susceptibility. The last step is a convolution of a spectrum as a function of the detuning with a Gaussian curve, which gives the theoretical spectral shape.

3. Experiment

The experimental setup is depicted in Figure 2. For the experiment we used a 25 mm long rubidium cell placed inside a solenoid. The measurements were made at room temperature (21°C). The magnetic shield made of high permeability metal was used to avoid

geomagnetic influence. The rectangular wave voltage from the generator was applied to the solenoid; the magnetic field was switched between B and $-B$ with a frequency 10–20 Hz. This relatively low frequency was taken to diminish the influence of the transition process on the results of the measurement. The beam of a tuneable semiconductor laser with plane output polarisation was expanded to approximately 5×8 mm size by a telescopic lens system. The 1 mm diameter aperture in front of the cell produced a circular beam with close to uniform intensity distribution. The photodetector with a small aperture in the centre of the beam was placed after the 45° tilted polariser. The lock-in amplifier was connected to the photodetector output. The laser frequency was scanned by steps across the line, and the lock-in output was monitored by a computer. The lock-in output signal is directly proportional to the Faraday rotation magnitude. Absorption is also affected by the magnetic field, but from symmetry arguments it follows that the absorption in our geometry does not change, when the magnetic field changes the sign, thus no signals due to absorption are detected by the lock-in. We checked this experimentally by measuring the lock-in signal without the polariser in front of the photodetector. The magnetic field induced circular dichroism is also present, but for small changes in polarisation state it does not manifest itself for our setup. It can be measured by placing a quarter-wave plate in front of the polariser, and has a magnitude comparable to that for optical rotation. The spectral dependences of this effect are reproduced by the theory as well, but we do not report them here.

The results of experiment are presented in Figure 3. It is seen that the calculation gives quite a satisfactory description for the complicated spectrum behaviour for all lines. For the open transitions the rotation signs are different for small and big magnetic fields. For big enough magnetic field, the lineshape can be strongly distorted from a nearly Gaussian form. In the ^{87}Rb $F_g = 1$ transition, the change of sign inside the line is possible. This occurs because the rotation directions from $F_e = 0, 1$ and $F_e = 2$ are opposite, and close to zero overall rotation corresponds to a situation when the sum is close to zero.

Thus, the rotation can be positive in one part of the line, and negative in another. For the ^{85}Rb $F_g = 2$ line, the distortion for the small overall rotation has another type, with two zero crossings. For stronger magnetic fields, there is a noticeable rotation between the two resolved lines of ^{85}Rb and line widening. The strong field effects result from a non-diagonal character of the magnetic field operator in a basis of eigenfunctions corresponding to a full atomic momentum F. These features are not reproduced correctly by the theory

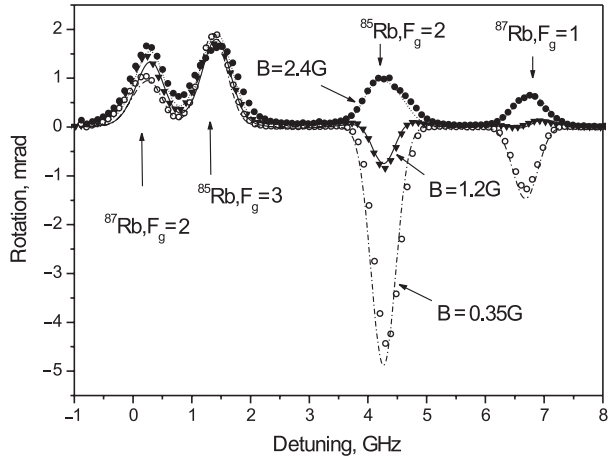

Figure 3. Theory (lines) and experiment (points) for light intensity $I = 1.1\,\mathrm{mW\,cm^{-2}}$, beam diameter 1 mm, temperature 21°C, and different magnetic fields. The only fitting parameter is a vapour density, common for all magnetic field values.

when the small field approximation is used for Zeeman splitting of the F-levels, though this approximation gives good estimations for peak values.

We did not perform measurements with high precision, in particular the cell did not have an antireflection coating, and there was around 20% variation in intensity across the input aperture. We estimate the systematic experimental error at 5–10% of maximal rotation amplitude. Nevertheless, the agreement between the theory and experiment is rather good, and all characteristic features, such as line widening, shape distortion and zero crossings are qualitatively reproduced by the theory.

References

[1] Budker, D.; Gawlik, W.; Kimball, D.F.; Rochester, S.M.; Yashchuk, V.V.; Weis, A. *Rev. Mod. Phys.* **2002,** *74,* 1153–1201.
[2] Korneev, N.; Benavides, O. *JOSA B* **2008,** *25,* 1899–1906.
[3] Siddons, P.; Adams, C.A.; Ge, C.; Hughes, I.G. *J. Phys. B* **2008,** *41,* 155004.
[4] Steck, D.A. Rubidium 85 D Line Data and Rubidium 87 D Line Data. http://steck.us/alkalidata (accessed May 14, 2009).
[5] Louisell, W.H. *Quantum Statistical Properties of Radiation*; Wiley: New York, 1973.
[6] Agarwal, G.S. *Quantum Statistical Theories of Spontaneous Emission and their Relation to Other Approaches*; Springer Tracts in Modern Physics 70, Springer Verlag: Berlin, 1974.
[7] Mølmer, K.; Castin, Y.; Dalibard, J. *J. Opt. Soc. Am. B* **1993,** *10,* 524–538.
[8] Rochester, S.M.; Hsiung, D.S.; Budker, D.; Chiao, R.Y.; Kimball, D.F.; Yashchuk, V.V. *Phys. Rev. A* **2001,** *63,* 043814.

[9] Plenio, M.B.; Knight, P.L. *Rev. Mod. Phys.* **1998,** *70,* 101–144.
[10] Agrawal, G.P. *Nonlinear Fiber Optics (Optics and Photonics)*, 3rd ed.; Academic Press: San Diego, 2001.

Appendix 1

We start with the equation

$$\partial_t \rho = -\frac{1}{2}(P\rho + \rho P) + \sum_{q=-1,0,1} C_q \rho C_q^+.$$

Using this, and relations for raising and lowering operators $C_q C_s = C_q^+ C_s^+ = 0$ and $PC_q = C_q^+ P = 0$ the second derivative of ρ is:

$$\partial_t^2 \rho = \frac{1}{4}(P^2\rho + 2P\rho P + \rho P^2) - \frac{1}{2}\sum_{q=-1,0,1} C_q(P\rho + \rho P)C_q^+.$$

Consequent calculation of derivatives and application of Taylor series

$$\rho(t+\Delta t) = \rho(t) + \partial_t \rho(t)(\Delta t) + \partial_t^2 \rho(t)\frac{(\Delta t)^2}{2!}\ldots$$

gives, after collecting the terms, Equation (7).